



# CHORUS

This is the accepted manuscript made available via CHORUS. The article has been published as:

## Drift and pseudomomentum in bounded turbulent shear flows

W. R. C. Phillips

Phys. Rev. E **92**, 043003 — Published 5 October 2015

DOI: [10.1103/PhysRevE.92.043003](https://doi.org/10.1103/PhysRevE.92.043003)

# Drift and pseudomomentum in bounded turbulent shear flows

W. R. C. Phillips\*

*Department of Mathematics, School of Science, Swinburne University of Technology, Hawthorn, Vic 3122, Australia*

(Dated: August 7, 2015)

This paper is concerned with the evaluation of two Lagrangian measures which arise in oscillatory or fluctuating shear flows when the fluctuating field is rotational and the spectrum of wavenumbers which comprise it is continuous. The measures are the drift and pseudomomentum. Phillips (*J. Fluid Mech.*, **430**, 2001) has shown that the measures are, in such instances, succinctly expressed in terms of Lagrangian integrals of Eulerian space-time correlations. But they are difficult to interpret and the present work begins by expressing them in a more insightful form. This is achieved by assuming the space-time correlations are separable as magnitude, determined by one-point velocity correlations, and spatial diminution. The measures then parse into terms comprised of the mean Eulerian velocity, one-point velocity correlations and a family of integrals of spatial diminution, which in turn define a series of Lagrangian time and velocity scales. The pseudomomentum is seen to be strictly negative and related to the turbulence kinetic energy, while the drift is mixed and strongly influenced by the Reynolds stress. Both are calculated for turbulent channel flow for a range of Reynolds numbers and appear, as Reynolds number increases, to approach a terminal form. At all Reynolds numbers studied the pseudomomentum has a sole peak located in wall units in the low teens while at the highest Reynolds number studied,  $Re_\tau = 5200$ , the drift is negative in the vicinity of that peak, positive elsewhere and largest near the rigid boundary. In contrast the time and velocity scales grow almost logarithmically over much of the layer. Finally, the drift and pseudomomentum are discussed in the context of coherent wall layer structures with which they are intricately linked.

## I. INTRODUCTION

Fluctuating fluid motions manifest in their simplest form as waves and at their most complicated as turbulence. In turn, the fluctuations interact to realize a further Lagrangian motion which goes by various labels; the one we use is ‘drift’. Physically, drift expresses the mean mass transport in excess (or deficit) of any Eulerian mean flow, while pseudomomentum determines the force exerted by the wave on the medium; both are wave properties [1]. Mathematically, drift and pseudomomentum are averaged measures of the quadratic interaction of fluctuations both with themselves (wave-wave) and any mean flow (wave-mean). Precise definitions arise in Andrews & McIntyre’s [2] generalized Lagrangian mean (GLM) formulation and these were used by Phillips [3] to evaluate the drift and pseudomomentum in discrete and continuous spectra of rotational waves in the presence of a strong shear flow. This paper is concerned with parsing those complicated expressions into a more insightful form and evaluating them in turbulent channel flow.

Drift arises in many circumstances in the physical sciences and is perhaps best known to fluid dynamists as Stokes drift [4]. But often overlooked is that Stokes was concerned with irrotational monochromatic surface waves in quiescent surroundings where only the first (wave-wave) interaction is active. This is the classic Stokes drift. On the other hand when the second (wave-mean) interaction plays a role the fluctuating field is more

likely rotational and the ensuing drift profile markedly different from the classic profile [5, 6]. One label for this case is the generalized Stokes drift [2, 3]; another is steady streaming [7]. Neither labels have gained traction and so we and others [6, 8] defer to the generic physics term, drift.

The drift and pseudomomentum are defined in terms of correlations that involve velocity fluctuations of a fluid particle and its displacement from a defined mean position [2] and can, for single wave trains, be evaluated in closed form. That said, the complexity of the calculation increases when the waves interact with an aligned shear flow, from zero or weak shear [4, 9], to moderate shear [6], to strong shear [10, 11]. Evaluation of the correlations poses even further difficulty for a spectrum of waves, even a discrete symmetric spectrum of irrotational waves in weak shear [12] and is formidable for a similar spectrum of rotational waves in strong shear [3]. Rather, in such instances it is expeditious to re-express the aforementioned correlations in terms of velocity correlations or, more precisely since we are concerned with Lagrangian measures, Lagrangian integrals of Eulerian space-time correlations.

Attempts to achieve this for a turbulent shear flow date from Lumley [13] and Phillips [14, 15]. But their results are clouded by secular behaviour and further progress with this approach stalled until Phillips [3], with insight gleaned from related work with single wave trains [16, 17], exposed the source of the secularities.

To do so he [3] employed GLM theory [2] to describe a clearly defined simpler (though not simple) problem, that of a train of small amplitude temporal 3D-waves riding on and interacting with a strong mean shear flow. GLM is ideal here because it parses fluid motion into un-

---

\* University of Illinois at Urbana-Champaign, Urbana, IL 61801-2935, USA. wrphilli@illinois.edu

ambiguous mean and oscillatory parts, thereby yielding precise definitions for the pseudomomentum and drift. The ensuing analysis is challenging but, amongst other things, it dictates the precise form the drift and pseudomomentum must take when specified in terms of well behaved Lagrangian integrals of space-time correlations.

That said, space-time correlations are difficult to acquire and those available are not broad enough to calculate the drift and pseudomomentum. In view of this, Phillips [18] developed a model for two point two-time velocity correlations and used it [3] to calculate the drift and pseudomomentum in turbulent channel flow for  $Re_\tau = 180$ . He found that the drift is oriented in the flow direction (that is positive) only near the wall with a zero at around thirteen wall units, while the pseudomomentum peaks near the zero in drift and is never positive. But whether these findings carry over to higher Reynolds numbers is unclear. Unclear too is the importance of these wave properties in turbulent flow and our aim herein is to resolve both questions.

Our motivation for doing so comes from several quarters, all related to how best characterize the structure of turbulent flows. The first reaches back to the work of Kraichnan and his Lagrangian perturbation theory [19, 20], from which he shows that a Lagrangian representation has the advantage of capturing more physics than an Eulerian one [21, 22]. If this finding is ubiquitous, then drift and pseudomomentum should likewise capture more of the physics than one-point Eulerian velocity correlations. Kraichnan’s perturbation theory and GLM are, of course, not identical, but there are connections. At the heart of his theory is a particular representation of Lagrangian motion which restricts attention to a generalized velocity field  $\mathbf{u}(\mathbf{x}, t|s)$ , defined as the velocity measured at time  $s$  in a fluid element which passes through  $\mathbf{x}$  at time  $t$  [19]. In contrast GLM invokes the traditional Lagrangian representation [2] and rests upon an exact mapping [23] of Navier Stokes (NS) into a Lagrangian mean reference frame to realize the Galilean invariant GLM-equations, which are then solved side by side with NS [3, 16]. To utilize them we employ perturbation expansions both for the Eulerian and Lagrangian-mean velocity fields [17]. Kraichnan, on the other hand, constructs two heuristic approximations within the framework of his generalized velocity field, *viz* the Lagrangian history direct interaction and an abridged version thereof, both of which are Galilean invariant and result as the lowest order of a systematic renormalization perturbation theory [24]. Thus whereas Kraichnan’s construct begins with perturbation theory, GLM begins with formal equations of motion which perturbation expansions then approximate.

Our second motivation has to do with the use of periodic Poiseuille flow as a metaphor for naturally occurring turbulent channel flow. Periodic Poiseuille flow is pressure driven laminar flow between parallel horizontal plates subjected to waves traveling in the flow direction. The flow is doubly periodic (streamwise and spanwise)

and as Reynolds number increases the interaction is unstable first to two and subsequently three dimensional waves [25] whose amplitudes grow until inhibited by nonlinearities, at which point the flow equilibrates [26, 27]. Of note is that the equilibrated flow comprised of 24 modes spanwise and streamwise “reflect(s) the basic integral properties of turbulent flows rather well” [26]. In fact only 16 modes are necessary to ensure the mean velocity profile depicts logarithmic behavior [27]. Thus since key mean features of turbulent channel flow are admirably described by periodic Poiseuille flow, which can be precisely described by Lagrangian mean field theory through GLM, an obvious progression is to exploit GLM to analyze the flow. Phillips [3, 17] has crafted the relevant theory (CLg theory) for doing so but it requires the drift an pseudomomentum as input.

Our third motivation is concerned with the relationship between drift and coherent structures, these being robust, reoccurring concentrations of vorticity that form near boundaries in turbulent shear flows and live over timescales long with respect to the fluctuating motions. The structures are characterized by velocity perturbations in the streamwise direction, known as streaks, and cross-stream perturbations which realize streamwise rolls; streaks and rolls together comprise a streamwise vortex. The association of the drift with these vortices is twofold: first, the vorticity (vortex lines) from which they form moves at the Lagrangian mean velocity, given by the sum of the Eulerian mean velocity and the drift; second, mean shear and differential drift act to effect the redistribution of vorticity necessary to the formation of the vortices.

Studies by Waleffe and coworkers [28–33] further indicate that such structures are self-sustaining, in the sense that streaks spawn rolls which in turn spawn streaks, the process being an integral feature of turbulent shear flows. Specifically, building on the work of Nagata [34], they question whether the equations describing simple parallel shear flows might support mutually coexistent wave and vortex systems, in the sense that the waves occur as instabilities of streamwise vortex flows with the waves ultimately large enough to drive the vortex flow, the process being self sustaining. They find not only that such a process can occur but that it is described by exact nonlinear solutions to the equations of motion. In spite of their importance though, the computation of ‘exact coherent states’ is a challenge, first because the solutions are disconnected from the structureless base state and second because the velocity scales for the rolls and streaks are disparate.

In view of that, Hall & coworkers [35–38] employ asymptotic theory to elucidate the underlying physics of the self-sustaining process and find that it is a finite Reynolds number analogue of a Rayleigh vortex-wave interaction. They further find that asymptotic theory closely concurs with the full theory for exact coherent states not only at high but also at small Reynolds number [38, 39]. This finding is supportive of the im-

portance of vortex-wave interaction theory in turbulent shear flows and in accord with earlier numerical studies of equilibrated periodic Poiseuille flow. Indeed such numerical studies not only depict the self-sustaining process [27, 40], but also show that “plane wave modes are present in turbulent flow and ... play an important if not essential role in turbulent wall bounded flows” [41]. Clear then is the ubiquity of vortices and waves in bounded turbulent shear flows, and known too is the genesis of the waves, but although the above works assume the presence of vortices, their genesis is unknown.

Lagrangian mean field theory is, of course, also able to describe the self sustaining process [42], so if Kraichnan’s finding that a Lagrangian representation is able to capture more physics than an Eulerian one holds true, then the possibility exists that Lagrangian mean theory might go a key step further and expose the mechanism(s) by which the vortices form.

In the upper-ocean mean shear and differential drift form the basis for an instability to stadium sized vortices known as Langmuir circulation [12] and long appealing is that similar ingredients play a role in the etiology of wall layer structures in bounded turbulent flows [14]. Were that to be the case, then the instability mechanism giving rise to structure is not the weak shear CL2 mechanism [12] relevant to the upper ocean, but rather its cousin CLg [8, 17, 43] as it applies in strong shear. In strong shear, the velocity scale of the streaks far exceeds that of the rolls [10, 17], which means the streaks act to modulate the fluctuating field. Thus, while retaining the seminal idea of the Craik-Leibovich [12] work, the CLg instability is markedly different to CL2 [10, 11]. Accordingly the underlying theory is more complicated [17], a feature which, in addition to the aforementioned secularity, confronted those [14, 15, 44] who first sought to take such notions further. Craik [10] and Phillips & Shen [11] were the first to solve this theory analytically, albeit in an asymptotic limit in the simpler context of irrotational wave fields in uniform shear [10] and rotational wave fields in nonuniform shear [11]; others [5, 45, 46] have considered more complicated cases numerically. As mentioned above, CLg theory requires the drift and pseudomomentum as input.

We begin in Sec. 2 by stating Phillips’ (2001) expressions for drift and pseudomomentum and then review his [18] model for space-time correlations. The model assumes the Corrsin-Kovasznay conjecture (see Sec. II B) which says that space-time correlations are separable as one point velocity correlations and spatial diminution. In Sec. III we expand his integral measures in terms of the model. In doing so we find (Sec. III A) that the Lagrangian integrals of spatial diminution act to realize time or velocity scales, which together with one-point velocity correlations and mean velocity, lead to concise expressions for each measure. Since direct simulations of turbulent channel flow are now available to  $Re_\tau = 5200$  [47] we use them to calculate the drift and pseudomomentum (in Sec. IV B) and thus explore their dependence, and that of the time and velocity scales, on Reynolds

number. We discuss our findings and utilize them in CLg theory in Sec. 5.

## II. FORMULATION

Of interest are multiscale problems in which the time scale of the fluctuations is significantly less than the time scale over which the mean flow evolves and likewise much less than the time scale over which any structure evolves. So in constructing a mean field theory we average over the shortest scale. An example from turbulence modeling is Reynolds averaging. This is an Eulerian average and its strength is its simplicity, but if the fluctuating field is rotational, the mean field equations do not retain the conservative properties of NS [3]. This is not usually a limitation in turbulence modeling but it can be when studying structure. Why? because vortex lines move with the fluid, that is they move at the Lagrangian velocity, so the mean vorticity field from which structure evolves, moves at the Lagrangian mean velocity. Ideally then, we would prefer to study the evolving vortical field from a Lagrangian mean frame rather than from an Eulerian mean frame. The velocity difference between the two mean frames is the drift.

The presence of drift in water waves was first exposed by Stokes [4], who expressed the Lagrangian velocity  $u_i^\xi$  (with components  $i = 1, 2, 3$ ) of a particle initially at position  $\mathbf{x}$  that follows a path determined by the displacement  $\boldsymbol{\xi}(\mathbf{x}, t)$ , in terms of an Eulerian velocity field  $u_i(\mathbf{x}, t)$  as

$$u_i^\xi(\mathbf{x}, t) = u_i(\mathbf{x} + \boldsymbol{\xi}(\mathbf{x}, t), t). \quad (1)$$

Then for waves of slope  $\epsilon \ll 1$  and  $\boldsymbol{\xi} = O(\epsilon)$ , a Taylor series expansion yields:

$$u_i^\xi(\mathbf{x}, t) = u_i + \xi_j u_{i,j} + \frac{1}{2} \xi_j \xi_k u_{i,jk} + \dots \quad (2)$$

Averaging now over the time scale of the waves and noting that  $u_i$  may comprise mean  $\bar{u}_i$  and fluctuating  $\check{u}_i$  parts as  $u_i = \bar{u}_i + \check{u}_i$ , yields the Lagrangian mean velocity [17]

$$\overline{u_i^\xi} = \bar{u}_i + \overline{\xi_j \check{u}_{i,j}} + \frac{1}{2} \overline{\xi_j \xi_k \check{u}_{i,jk}} + \dots, \quad (3)$$

from which the drift  $d_i$  is evident as the difference between  $\overline{u_i^\xi}$  and  $\bar{u}_i$ , to wit

$$d_i = \overline{u_i^\xi} - \bar{u}_i = \overline{\xi_j \check{u}_{i,j}} + \frac{1}{2} \overline{\xi_j \xi_k \check{u}_{i,jk}} + \dots \quad (4)$$

Observe that the drift is a second-order averaged wave-wave property, which reduces to the Stokes drift when  $\bar{u}_i = 0$ .

Accordingly, if we apply the same mapping  $\mathbf{x} \mapsto \mathbf{x} + \boldsymbol{\xi}$  and Lagrangian average to NS we obtain (after some work, see [2, 23]) mean field GLM equations for  $\overline{u_i^\xi}$  that retain the conservative properties of NS. Inherent therein

is a further second-order averaged wave-wave property, the pseudomomentum [2]

$$p_i = -\overline{\xi_{j,i} u_j^\ell}, \quad (5)$$

where  $u_j^\ell = \check{u}_j + \xi_k \bar{u}_{j,k}$  [17]. Finally, note that while  $d_i$  and  $p_i$  are quadratic averages of the interacting fluctuating velocity  $\check{u}_j$  and displacement fields  $\xi_j$ , and are specified by GLM, the fields  $\check{u}_j$  and  $\xi_j$  themselves are necessarily solutions to NS given  $\bar{u}_i$  and appropriate boundary conditions. Examples in which  $\check{u}_j$ ,  $\xi_j$  and  $d_i$ ,  $p_i$  are determined for given  $\bar{u}_i$  can be found in [11, 16, 17].

### A. Lagrangian measures in terms of space-time correlations

Phillips [3] considers a fluctuating finite amplitude three-dimensional disturbance defined by a spectrum of wavenumbers riding on a parallel Eulerian mean shear flow  $U(z)$  of constant density aligned in the  $x$  direction with  $y$  cross stream. All variables are rendered dimensionless with respect to appropriate characteristic length, velocity and time scales, an example of which is given in Sec. IV B. He derives Eqs. (4) and (5) for the drift  $D_i$  and pseudomomentum  $P_i$  as defined in GLM theory [2] for both discrete and continuous spectra. Of interest here is the latter case, for which the streamwise components  $D_1(z)$  and  $P_1(z)$  are:

$$D_1 = -\frac{\partial}{\partial z} \int_0^{\tau^*} Q_{31} d\tau - \frac{1}{2} \frac{d^2 U}{dz^2} \int_{\tau^*}^0 \int_0^\zeta Q_{33} d\tau d\zeta \quad (6)$$

and

$$P_1 = \int_0^{\tau^*} \frac{\partial}{\partial r} Q_{jj} d\tau + \frac{dU}{dz} \int_{\tau^*}^0 \int_0^\zeta \frac{\partial}{\partial r} (Q_{31} - Q_{13}) d\tau d\zeta + \left(\frac{dU}{dz}\right)^2 \int_{\tau^*}^0 \int_0^\chi \int_{\tau^*}^\zeta \frac{\partial}{\partial r} Q_{33} d\tau d\zeta d\chi. \quad (7)$$

Herein  $Q_{ij}$  are space-time correlations at time delay  $\tau$  and spatial delay  $r = U\tau$  (see below) while  $\zeta$  and  $\chi$  are dummy variables for  $\tau$ . Finally  $\tau^*(z)$  is a unique value of  $\tau$  determined by an integral constraint discussed in Sec. II B.

### B. Space-time correlations

To evaluate Eqs. (6) and (7) we require  $U$  and  $Q_{ij}$ . The mean flow  $U$ , of course, is easily acquired but that is not the case for the two-point two-time Eulerian space-time correlation  $Q_{ij}$ .  $Q_{ij}$  is defined as [48]

$$Q_{ij}(\mathbf{x}; \mathbf{r}, \tau) = \overline{u_i(\mathbf{x}, t) u_j(\mathbf{x} + \mathbf{r}, t + \tau)}, \quad (8)$$

where  $\mathbf{u}(\mathbf{x}, t) = u_i(\mathbf{x}, t)$  is the velocity of the flow with components  $(u, v, w)$  at point  $\mathbf{x} = (x, y, z)$  at time  $t$ , with

$\mathbf{r}$  and  $\tau$  respective displacements therefrom, while  $\overline{(\cdot)}$  denotes averaging over sufficient time to render the average statistically stationary.

Because of the complexity in determining  $Q_{ij}$ , and dearth of examples of it [49, 50], Phillips [18] chose to model it. His model is based upon the Kovasznay-Corrsin [51, 52] conjecture, which is in essence that  $Q_{ij}$  is separable as magnitude, set by the one point velocity correlation  $\overline{u_i u_j}$  and the then unity normalized correlation  $R_{ij}$ , yielding

$$Q_{ij}(\mathbf{x}; \mathbf{r}, \tau) = \overline{u_i u_j}(\mathbf{x}) R_{ij}(\mathbf{x}; \mathbf{r}, \tau). \quad (9)$$

The conjecture further states that  $R_{ij}$  may be expressed solely in terms of spatial diminution, a simplification Kraichnan [53] showed to be valid provided  $R_{ij}$  is an appreciable fraction of unity; a feature well supported experimentally [49] and by DNS [50]. Indeed the available DNS data is supportive of the approximation of Eq. (8) by Eq. (9) across the full range of  $R_{ij}$ . Finally, in applying the conjecture we must also ensure that  $R_{ij}$  satisfies formal asymptotic limits for small and large displacements [18].

Of interest in our present study are mean shear flows that evolve gradually (or not at all) in  $x$  and are statistically stationary in  $y$ , rendering  $\partial(\cdot)/\partial x \approx \partial(\cdot)/\partial y = 0$ . This means  $\overline{u_i u_j}$  is a function solely of  $z$  while  $Q_{ij}$  depends on  $z$  and  $\mathbf{r}$ , so that  $Q_{ij}(\mathbf{x}; \mathbf{r}, \tau) \mapsto Q_{ij}(z; \mathbf{r}, \tau)$ . Furthermore because Eqs. (6) and (7) require space-time correlations at delay  $\mathbf{r} = (r, 0, 0)$ , the subset of correlations of interest here are

$$Q_{ij}(z; \mathbf{r}, \tau) = \overline{u_i u_j}(z) R_{ij}(U\tau, 0, 0, \tau). \quad (10)$$

Note that the correlations are not at optimal delay, which would require that  $U = V$ , where  $V$  is the mean velocity at which  $\partial R_{ij}/\partial r = 0$ , although away from a rigid boundary  $V \approx U$  [50]. Accordingly  $V$  is not equivalent to the Lagrangian mean velocity  $U + D_1$ .

To evaluate Eq. (10) we require  $U$ ,  $\overline{u_i u_j}$  and  $R_{ij}$ . Details of  $U$  and  $\overline{u_i u_j}$  are available for specific Reynolds numbers from direct simulations (see Sec. IV B) and any Reynolds number from asymptotically correct integral expressions for boundary layer and channel flows [54–56]. The correlation  $R_{ij}$  and how to evaluate it, on the other hand, are given in [18].

That said, it is expeditious to discuss  $\tau^*$ . We do so from the viewpoint of a simple example given by [3], who notes that the correlations  $R_{ij}$  have the generic form  $\mathcal{R}$  say, as

$$\mathcal{R}(\eta) = (1 + C\eta)^{-\frac{3}{2}}, \quad (11)$$

where  $\eta \propto \tau$  and  $C$  is constant. To exclude spurious behavior,  $\mathcal{R}$  and integrals of  $\mathcal{R}$  must satisfy several constraints, the first being that  $\mathcal{R}(1) = \frac{1}{2}$ , which requires that  $C = 0.5874$ . The second, that

$$\int_0^{\eta^*} \mathcal{R}(\eta) d\eta = 1, \quad (12)$$

requires  $\eta^* = 1.7102$  and thereby defines  $\tau^*$ . The remaining constraints are concerned with specifying integration limits on multiple integrals, specifically to ensure double integrals have their first zero at  $\eta = \eta^*$ , while triple integrals are zero at  $\eta = 0$ . These dictate the limits specified in Eqs. (6) and (7).

From this point we assume  $U$ ,  $\overline{u_i u_j}$  and  $R_{ij}$  are known, and proceed to express  $D_1$  and  $P_1$  in terms of them.

### III. DRIFT AND PSEUDOMOMENTUM

#### A. Approximations

We begin by substituting Eq. (10) into Eq. (6) to find

$$-D_1(z) = \frac{d\overline{uw}}{dz} \int_0^{\tau^*} R_{31} d\tau + \overline{uw} \frac{d}{dz} \int_0^{\tau^*} R_{31} d\tau + \frac{\overline{w^2}}{2} \frac{d^2 U}{dz^2} \int_{\tau^*}^0 \int_0^\zeta R_{33} d\tau d\zeta. \quad (13)$$

Observe that the separability introduced in Eq. (9) allows each term to be parsed into an Eulerian mean portion and a Lagrangian integral which, in turn, defines a  $z$ -dependent integral scale. Specifically Eq. (13) exposes two integral time scales  $\mathcal{A}$  and  $\mathcal{B}$  as

$$\mathcal{A} = \int_0^{\tau^*} R_{31} d\tau \quad \text{and} \quad \mathcal{B}^2 = -\frac{1}{2} \int_{\tau^*}^0 \int_0^\zeta R_{33} d\tau d\zeta. \quad (14)$$

Turning now to  $P_1$  we proceed the same way, albeit term by term. Here, on substituting Eq. (10) into the first term in Eq. (7) yields

$$\frac{\partial Q_{jj}}{\partial r} = \overline{u^2} \frac{\partial R_{11}}{\partial r} + \overline{v^2} \frac{\partial R_{22}}{\partial r} + \overline{w^2} \frac{\partial R_{33}}{\partial r} \quad (15)$$

which we write as

$$-\int_0^{\tau^*} \frac{\partial Q_{jj}}{\partial r} d\tau = \frac{\overline{u^2}}{\mathcal{U}} + \frac{\overline{v^2}}{\mathcal{V}} + \frac{\overline{w^2}}{\mathcal{W}}, \quad (16)$$

where the velocity scales  $\mathcal{U}$ ,  $\mathcal{V}$  and  $\mathcal{W}$  are

$$[\mathcal{U}^{-1}, \mathcal{V}^{-1}, \mathcal{W}^{-1}] = -\int_0^{\tau^*} \frac{\partial R_{jj}}{\partial r} d\tau. \quad (17)$$

Note that because  $R_{ij}$  is by definition unity when  $\tau = 0$  and must decrease eventually to zero as  $\tau$  increases, we expect  $\partial R_{ij}/\partial r$ , and in turn the integrals on the right hand side of Eqs. (14) and (17), to be largely negative. For that reason we have introduced a negative sign to render the scales positive.

Looking now at the second term in Eq. (7), we find the difference  $Q_{31} - Q_{13}$ . Since modelling [18] requires  $Q_{ij} = Q_{ji}$  we neglect this term. Lastly, since  $Q_{33} = \overline{w^2} R_{33}$ , we find that the triple integration in the third term in Eq. (7)

gives rise to the integral time scale  $\mathcal{C}$  defined relative to a velocity scale, which we choose to be  $\mathcal{W}$ , yielding

$$\mathcal{C}^2 = -\mathcal{W} \int_{\tau^*}^0 \int_0^\chi \int_{\tau^*}^\zeta \frac{\partial}{\partial r} R_{33} d\tau d\zeta d\chi. \quad (18)$$

Finally, our approximations for Eqs. (6) and (7) are

$$-D_1 = \frac{d}{dz} (\mathcal{A} \overline{uw}) + \mathcal{B}^2 \overline{w^2} \frac{d^2 U}{dz^2} \quad (19)$$

and

$$-P_1 = \frac{\overline{u^2}}{\mathcal{U}} + \frac{\overline{v^2}}{\mathcal{V}} + \frac{\overline{w^2}}{\mathcal{W}} \left[ 1 + \left( \mathcal{C} \frac{dU}{dz} \right)^2 \right]. \quad (20)$$

To this point Eqs. (19) and (20) apply to any turbulent shear flow that varies slowly in  $x$  and is statistically stationary in  $y$ , be it bounded or unbounded in  $z$ . We further note that since all terms on the right hand side of Eq. (20) are strictly positive that the pseudomomentum is necessarily negative, a feature we will discuss in Sec. V.

Details of the drift given by Eq. (19) on the other hand are less clear, in that the terms are of mixed sign, so that  $D_1$  may well be mixed. What is clear from Eq. (19) though is the dependence of  $D_1$  on the closely related quantities  $U$  and  $\overline{uw}$ . For example, in channel flow with rigid boundaries at  $z = 0$  and  $z = 2\delta$ , the interdependence of  $\overline{uw}$  and  $U$  follows from the mean streamwise momentum equation, which reduces to

$$0 = \frac{1}{\delta} + \frac{d^2 U}{dz^2} - \frac{d\overline{uw}}{dz}, \quad (21)$$

allowing us to express Eq. (19) in terms of  $\overline{uw}$  or  $U$  (see Sec. V). Indeed since  $U$  and  $\overline{u_i u_j}$  are well known for a range of classic turbulent flows, it is straightforward to evaluate Eqs. (19) and (20) provided we have a clear idea of the behaviour of the time and velocity scales, something we address in Sec. IV D.

## IV. RESULTS - CHANNEL FLOW

### A. Background

Phillips [3] gave only one example of  $D_1$  and  $P_1$ , that being for turbulent channel flow at  $\text{Re}_\tau = 180$ . With the arrival of petascale computing, however, direct simulations are now available to  $\text{Re}_\tau = 5200$  [47]. Moreover, computations at some of the lower Reynolds numbers, namely  $\text{Re}_\tau = 180, 550, 950$  and  $2000$  [by respectively, 57–60], have been recomputed at higher resolution [by 47]. In calculating further examples of drift and pseudomomentum, therefore, we employ Lee & Moser's results at  $\text{Re}_\tau = 180, 550, 1000, 2000$  and  $5200$ , with [61] at  $\text{Re}_\tau = 4200$ .

Our examples are given in terms of wall units, which defer to length  $\nu/\tilde{U}_\tau$  and time  $\nu/\tilde{U}_\tau^2$  scales, linked by the

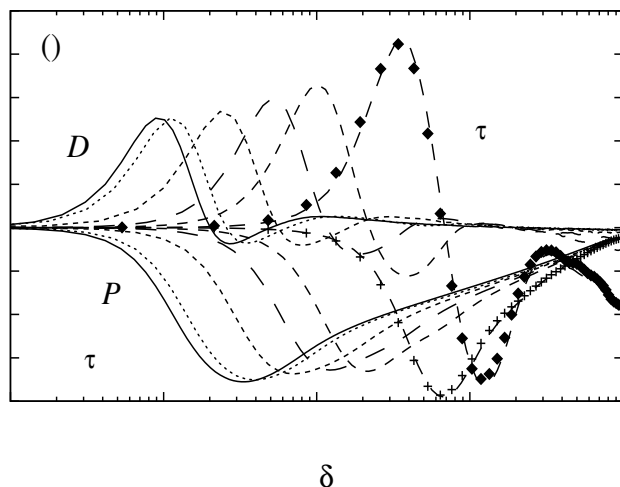
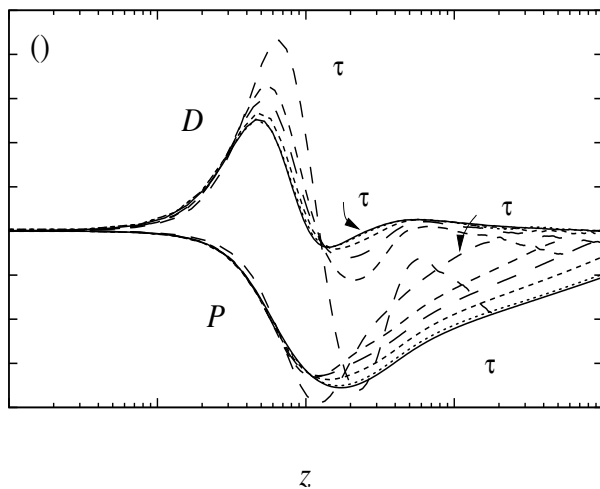


FIG. 1. Profiles of drift  $D_1$  and pseudomomentum  $P_1$  as a function of distance from the boundary in: (a) wall units and (b) outer units. The profile are for turbulent channel flow for  $Re_\tau = 180, 550, 1000, 2000, 4200$  and  $5200$ ; previous calculations of  $D_1$   $\blacklozenge$  and  $P_1$   $+$  at  $Re_\tau = 180$  by [3].

friction velocity  $\tilde{U}_\tau = (\nu d\tilde{U}/d\tilde{z}|_{\text{wall}})^{\frac{1}{2}}$ . Then  $\delta = \delta\tilde{U}_\tau/\nu = Re_\tau$ , where  $\nu$  is the kinematic viscosity of the fluid. For convenience we set  $z = 0$  at the wall and consider flow in the region  $z \in [0, \delta]$ . Such normalization is often highlighted by the superscript  $+$ , but we forgo that noting that Eqs. (6) and (7), and expressions which follow them, are not affected by details of the normalization. Moreover all variables used hitherto are nondimensional, with the exception of  $\tilde{U}$ ,  $\tilde{z}$  and  $\tilde{\delta}$ .

## B. Reynolds number dependence

Our first task is to deduce the dependence of drift and pseudomomentum on Reynolds number and thus plot results at all  $Re_\tau$  in Fig. 1. These are plotted both in wall

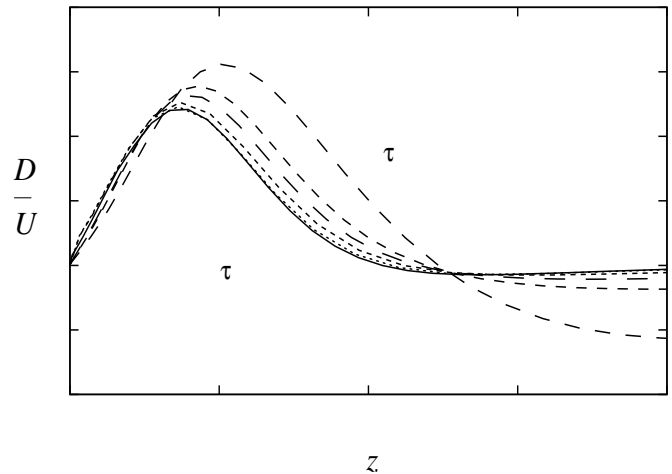


FIG. 2. Profiles of drift  $D_1$  relative to the mean velocity  $U$  with distance  $z$  from the boundary in wall units for  $Re_\tau = 180, 550, 1000, 2000, 4200$  and  $5200$ .

units (Fig. 1(a)) and outer units (Fig. 1(b)), where the independent variable is  $z/\delta$ . We also include Phillips' [3] previous findings, which concur well with the more highly resolved results at  $Re_\tau = 180$ .

Looking first at the drift with increasing distance from the wall in wall units, we observe collapse, or close to it, for all  $Re_\tau$  only in the viscous sublayer. Each profile then goes on to a peak, a peak that is positive and diminishes with increased  $Re_\tau$ . Profiles for all  $Re_\tau$  then intersect at much the same location  $z = z_f \in (13, 14)$ . Furthermore, since the drift is negative at  $z_f$  all profiles necessarily exhibit a zero at  $z < z_f$ . A second peak, this one negative, occurs in the buffer layer near  $z \in (15, 25)$ ; this peak diminishes in magnitude and moves towards  $z_f$  as  $Re_\tau$  increases. Near  $z \in (30, 60)$ , as the buffer layer is transitioning to the logarithmic region, the profiles reach a third peak. This peak is positive for all cases except  $Re_\tau = 180$  and from it the drift varies monotonically to its centerline value, a value that is markedly negative at the lowest  $Re_\tau$  but essentially zero at the highest  $Re_\tau$ . Finally, while all profiles exhibit consistent behaviour across the channel domain, they appear to relax, as  $Re_\tau$  increases, to the profile at the highest  $Re_\tau$ . Indeed there is little difference between the curves at the two highest  $Re_\tau$ , with the inference that drift profile is asymptotic to a limiting form and that the  $Re_\tau = 5200$  results are close to that form, although only results at much higher  $Re_\tau$  can confirm it.

Just how significant the drift is relative to the Eulerian mean flow  $U$  is seen in Fig. 2, where we plot  $D_1/U$ . Again we see that while the drift is most active in the viscous sublayer and buffer layer regions, Reynolds number plays a clear role only in the later and diminishes as Reynolds number increases. Moreover since  $U$  is independent of Reynolds number in wall scaling in the inner region, these findings necessarily carry over to the Lagrangian mean

velocity  $U + D_1$ .

Returning now to Fig. 1(a) but turning to the pseudomomentum, we see that the profiles are much simpler than those for the drift and are, as anticipated in Eq. (20), always negative. Looking in more detail we find as  $z$  increases that, in contrast to the drift, collapse extends into the buffer layer, to approximately  $z = 10$ . The profiles peak in the vicinity of but not at  $z_f$  and then relax, irrespective of  $Re_\tau$ , to approximately the same non-zero centerline value. Finally, in line with our inference for the drift, the pseudomomentum profiles also appear to approach a terminal form as  $Re_\tau$  increases.

When viewed in outer units (Fig. 1(b)), on the other hand, the profiles for both measures are distinctly separate not only in the inner region as we would expect, but also in the outer region where our mindset is some degree of collapse. Of course each profile may be asymptotic to a distinct curve in the outer region and certainly a case for that can be made for the pseudomomentum, which depicts a clear logarithmic decay at the highest two Reynolds numbers, namely  $Re_\tau = 4200$  and  $5200$ .

Indeed, given that in the outer region the mean enstrophy

$$\left(\mathcal{E} \frac{dU}{dz}\right)^2 \ll 1, \quad (22)$$

we see that the pseudomomentum given by Eq. (20) is dominated by the variances of  $u$ ,  $v$  and  $w$ . We further know from Townsend's [48] attached eddy hypothesis, asymptotic analysis [54, 55] and numerous high Reynolds number experiments [62], that

$$\overline{u_i^2} = A_i - B_i \ln\left(\frac{z}{\delta}\right) \quad \text{for } (i = 1, 2, 3) \quad (23)$$

in the logarithmic region. Here  $B_3 = 0$  while the remaining  $A_i$  and  $B_i$  are positive constants whose values are well resolved experimentally [62]. Eq. (23) is captured by the DNS results only for  $v^2$ , with  $A_2 = 1.08$  and  $B_2 = .387$  [47]. Nevertheless, it is clear from Eq. (20) that the pseudomomentum will likewise exhibit logarithmic decay in the outer region.

### C. Component terms

In Fig. 3 we look at the contribution of each term to the drift Eq. (19) and pseudomomentum Eq. (20) at the highest Reynolds number  $Re_\tau = 5200$ . In fact we expand the first term in Eq. (19) and denote the resulting components by  $I$  and  $II$ , with the last term denoted by  $III$ . Consecutive terms in the pseudomomentum are labeled  $i - iv$ .

Components which comprise the drift are plotted in Fig. 3(a). Observe that  $I = -\mathcal{A} d\overline{uw}/dz$  is predominantly positive, with  $III$  strictly negative while  $II$  is mixed;  $D_1$  is given by the solid line. Interestingly, behaviour in the sublayer is determined almost exclusively by  $I$ , while  $II$

and  $III$  play key roles in the buffer layer. Simplification of Eq. (19) is thus not possible because although  $I$  is the dominant term, the absence of terms  $II$  and  $III$  would noticeably alter the profile for  $D_1$ .

Is that conclusion affected by Reynolds number? No, as we see in Fig. 4, where the first ( $I + II$ ) and last terms in Eq. (19) are plotted for a range of  $Re_\tau$ . Clearly each component is influenced by Reynolds number and that influence diminishes as  $Re_\tau$  increases, but the level of influence is much the same in each term.

In contrast all terms contributing to the pseudomomentum are, as we see in Fig. 3(b), strictly negative, with  $i$  the dominant term and  $iii = -\overline{w^2}/\mathcal{W}$  the least influential;  $P_1$  is given by a solid line. We further note that while all terms make a meaningful contribution to  $P_1$ , terms  $ii - iv$  do not hugely alter its profile from that given by term  $i$ , suggesting the simple approximation  $P_1 \propto \overline{u^2}/\mathcal{U}$ .

### D. Time and velocity scales

The mean velocity, variance and covariance collapse in the wall region, so the lack of collapse depicted by  $D_1$  and  $P_1$  in Fig. 1(a) in the wall region must, in view of Eqs. (19) and (20), reflect a Reynolds number dependence on the time ( $\mathcal{A}, \mathcal{B}, \mathcal{C}$ ) and velocity scales ( $\mathcal{U}, \mathcal{V}, \mathcal{W}$ ).

The time scales are plotted in Figs. 5(a) and 5(b), the former at  $Re_\tau = 180$  and the latter at  $Re_\tau = 5200$ . Observe that the value of each scale at  $z = 0$  and  $z/\delta = 1$  is little affected by  $Re_\tau$ . Moreover, all profiles are essentially constant in the sublayer the ultimately (in fact over much of the layer) grow with distance from the wall. But the profiles in the interior and specifically in the wall region, are affected by Reynolds number. This dependence is particularly evident in the differential of  $\mathcal{A}$ , as we observe in Fig. 6 although, in line with our earlier findings, it diminishes with increasing Reynolds number suggesting that  $\mathcal{A}$ ,  $\mathcal{B}$  and  $\mathcal{C}$  approach a terminal form.

Lastly we plot, in Figs. 7(a) and 7(b), the velocity scales at the lowest and highest  $Re_\tau$ . Here we find that although the scales have the same generic form, to wit initially constant and ultimately almost logarithmic, the details are very much Reynolds number related. For example the low Reynolds number results for  $\mathcal{U}$  and  $\mathcal{V}$  exhibit two regions of growth, while the higher ones do not. Also, in contrast to the time scales, the end values at  $z = 0$  and  $z/\delta = 1$  change significantly with Reynolds number. Interestingly though, much of that dependence is offset when the scales are utilized in Eq. (20) and all is summated to depict  $P_1$ .

## V. DISCUSSION

Our aim to express Phillips' [3] expressions for drift Eq. (6) and pseudomomentum Eq. (7) in a more insightful form was well achieved by invoking the Corrsin-

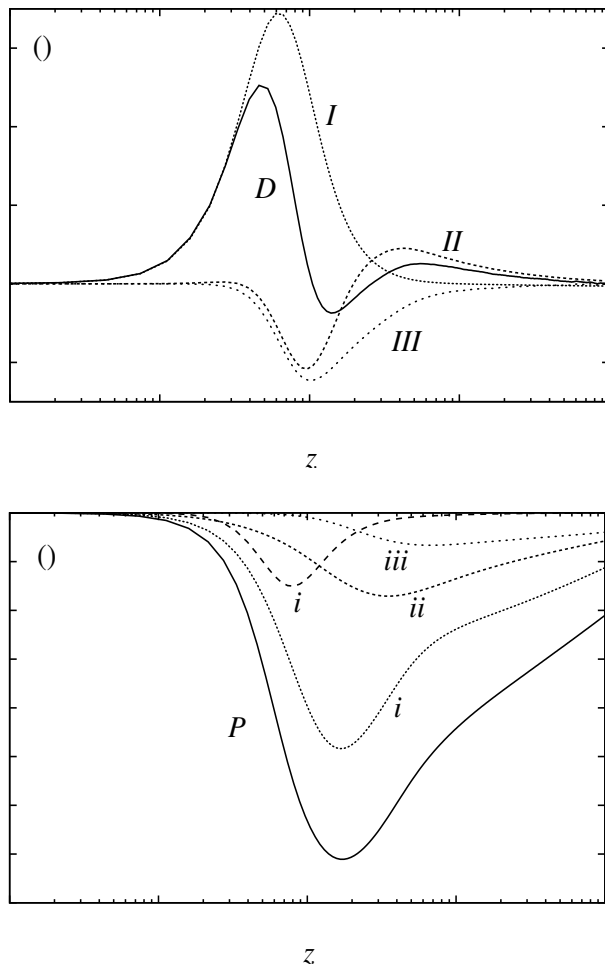


FIG. 3. Profiles of the component terms  $I$ ,  $II$  and  $III$  as defined in the text for (a) the drift  $D_1$  Eq. (19) and terms  $i$ ,  $ii$ ,  $iii$ ,  $iv$  for the (b) pseudomomentum  $P_1$  Eq. (20) as a function of distance  $z$  from the boundary in wall units, for channel flow for  $Re_\tau = 5200$ .

Kovaszny conjecture. The conjecture being that space-time correlations are separable as one point velocity correlations and spatial diminution. This means that the Lagrangian integrals of space-time correlations at the heart of Eqs. (6) and (7) are likewise separable as now familiar mean Eulerian variables premultiplying Lagrangian integrals of spatial diminution, which we conveniently mask as Lagrangian time and velocity scales. All is then known save the scales.

Even without knowledge of the scales it is likely that the drift Eq. (19) is mixed because terms which comprise it are mixed. To place this in perspective, drift in irrotational surface waves in the absence of imposed shear, like Stokes drift (see Sec. I), is positive; that is a Lagrangian mean velocity aligned in the direction of wave propagation [4, 9]. On the other hand irrotational or weakly rotational waves in the presence of moderate shear can lead to drift that is mixed [6], meaning that

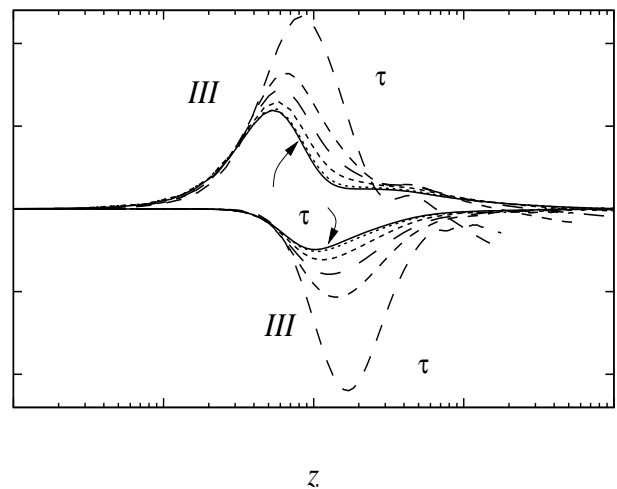


FIG. 4. Profiles of the first  $I + II$  and second  $III$  component terms of the drift  $D_1$  defined in Eq. (19) as a function of distance  $z$  from the boundary in wall units, for channel flow at  $Re_\tau = 180, 550, 1000, 2000, 4200$  and  $5200$ .

the Lagrangian mean velocity  $U + D_1$  can be less than or in excess of, the Eulerian mean flow  $U$ .

The drift is also mixed in turbulent channel flow, as we found in Sec. IV B. Specifically it is positive in the viscous sublayer, negative for much of the buffer region and, depending on the Reynolds number, mixed in the logarithmic and outer regions. These alternating layers of positive and negative drift are clearly evident in Fig. 1(a) along with the finding as Reynolds number increases, that the drift profile appears to approach a terminal form. At all Reynolds numbers, however, the drift is strongest immediately adjacent to the wall and is dominated in that region (see Sec. IV C) by terms  $I + II = -d\mathcal{A}\overline{uw}/dz$  (see Fig. 4) and in particular by  $I = -\mathcal{A}d\overline{uw}/dz$  (shown in Fig. 3(a)). Indeed because  $\overline{uw}$  plays such a key role in the drift it is instructive to write Eq. (19) in a manner which highlights  $\overline{uw}$ , viz

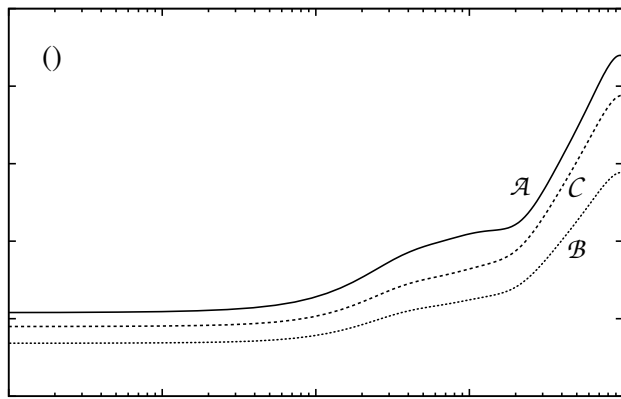
$$-D_1 = \frac{d\overline{uw}}{dz} (\mathcal{A} + \mathcal{B}^2 \overline{w^2}) + \overline{uw} \frac{d\mathcal{A}}{dz} - \frac{\mathcal{B}^2 \overline{w^2}}{\delta}, \quad (24)$$

or in terms of  $U$  as

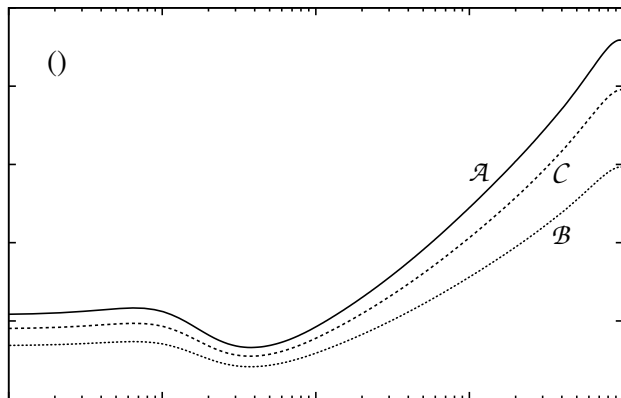
$$-D_1 = \frac{d^2 U}{dz^2} (\mathcal{A} + \mathcal{B}^2 \overline{w^2}) + \frac{dU}{dz} \frac{d\mathcal{A}}{dz} + \frac{d}{dz} \left[ \mathcal{A} \left( \frac{z}{\delta} - 1 \right) \right]. \quad (25)$$

That said, we emphasize that although the importance of the Reynolds stress  $\overline{uw}$  to the drift was not previously known, the importance of  $\overline{uw}$  to the mechanics of bounded turbulent shear flow and the presence of wall region structure, has long been known [64]. Of particular importance is its wall normal derivative and where that derivative is zero.

Its derivative is zero in the log region where large scale roll-mode structures are observed. These structures



$z \delta$



$z \delta$

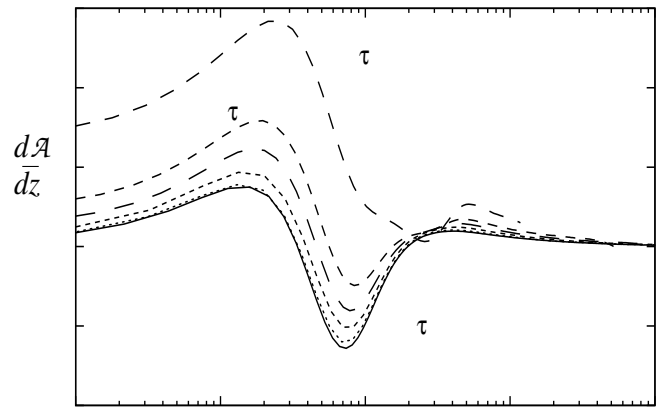
FIG. 5. Profiles of the time scales  $\mathcal{A}$ ,  $\mathcal{B}$ ,  $\mathcal{C}$  in wall units as a function of distance  $z$  from the boundary in outer units, for channel flow at (a)  $\text{Re}_\tau = 180$  and (b)  $\text{Re}_\tau = 5200$ .

would appear to not be closely coupled with their near wall counterparts, because they are also observed over rough walls, which obliterate structure close to the wall. Moreover we might identify them with one of two exact coherent state solutions, one adjacent to the wall and the other further out, admissible to the equations of motion in boundary layer flows [65].

Having considered the pseudomomentum in the log region (Sec. IV B), we look now to the drift, and note that because  $\overline{uw} \sim -1$  and  $\overline{w^2} \sim A_3$  there [48], that Eq. (24) reduces to

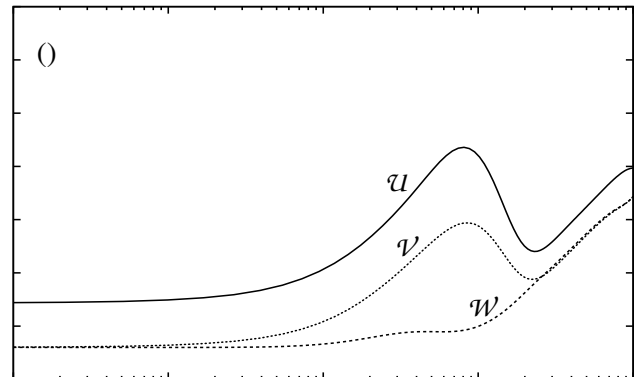
$$D_1 \sim \frac{d\mathcal{A}}{dz} + \frac{\mathcal{B}^2 A_3}{\delta}. \quad (26)$$

Furthermore in view of Figs. 5 and 6 we see that the second term in Eq. (26) dominates. So the drift then varies as  $\mathcal{B}^2$ , that is logarithmically with  $z$ , as does the pseudomomentum and mean velocity.

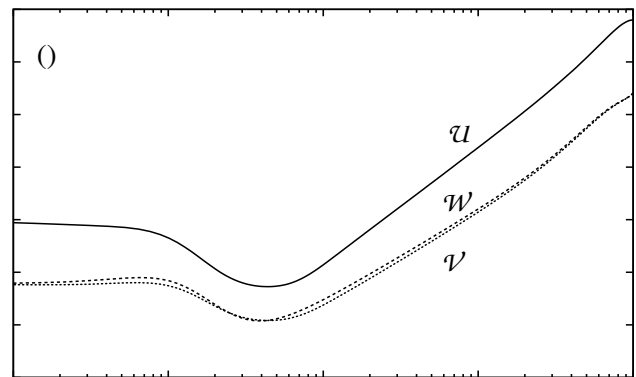


$z$

FIG. 6. Profiles of the differential time scale  $d\mathcal{A}/dz$  as a function of distance  $z$  from the boundary in wall units, for channel flow at  $\text{Re}_\tau = 180, 550, 1000, 2000, 4200$  and  $5200$ .



$z \delta$



$z \delta$

FIG. 7. Profiles of the velocity scales  $\mathcal{U}$ ,  $\mathcal{V}$  and  $\mathcal{W}$  in wall units as a function of distance  $z$  from the boundary in outer units for channel flow at (a)  $\text{Re}_\tau = 180$  and (b)  $\text{Re}_\tau = 5200$ .

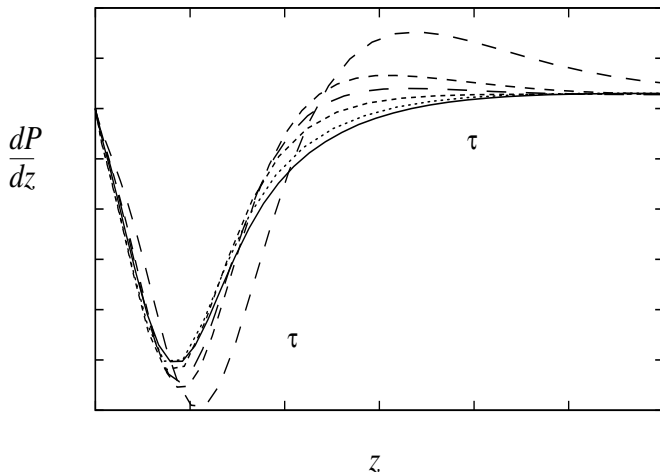


FIG. 8. Profiles of the differential pseudomomentum  $dP_1/dz$  with distance  $z$  from the boundary in wall units, for  $Re_\tau = 180, 550, 1000, 2000, 4200$  and  $5200$ .

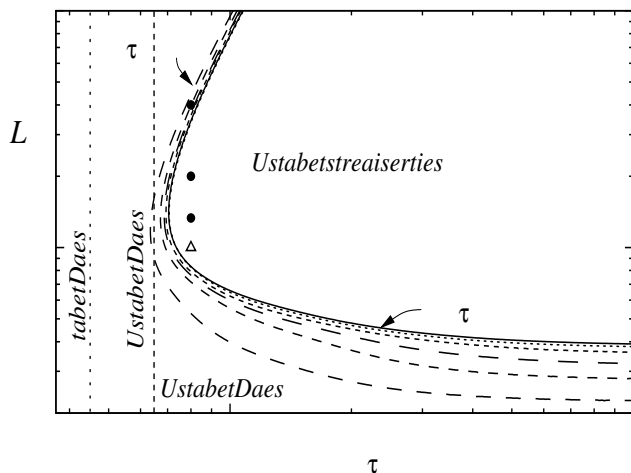


FIG. 9. Stability boundaries for the onset of streamwise vortex structure depicted by the linear steady states of CLg theory [17] describing periodic Poiseuille flow for  $Re_\tau = 180, 550, 1000, 2000, 4200$  and  $5200$ , expressed as vortex spacing  $L$  (2 rolls) in wall units against  $Re_\tau$ . The asymptotes for instability to two- and three-dimensional waves determined numerically are drawn at  $Re_\tau = 45$  and  $Re_\tau = 64.8$  [63]. Numerical results for  $\bullet$  Roll spacing and  $\triangle$  ensemble average of streak spacing at  $Re_\tau = 80$  [41].

In contrast to the drift, the pseudomomentum Eq. (20) is strictly negative throughout the layer, a result which concurs with findings for monochromatic rotational waves in flows with strong shear [5, 10, 11, 45, 46]. Is pseudomomentum always negative? No. In irrotational waves in the absence of shear it reduces to the Stokes drift [3] and is positive. Moreover since momentum appears

in the form of Stokes drift in irrotational surface gravity waves [1] we could equally say in that instance that pseudomomentum appears as momentum. But surface gravity waves are a special case. Waves do not usually have a uniquely defined mean momentum, which means the force (exerted by the waves on the fluid medium) must appear in the form of pseudomomentum. If the pseudomomentum is negative, then the force it acts to realize is opposed to the mean flow and acts to retard it. If fact when written as  $\mathcal{U}P_1$ , we see from Eq. (20) that pseudomomentum is akin to the turbulence kinetic energy  $\overline{u^2 + v^2 + w^2}$ .

How though do the drift and pseudomomentum affect the etiology of wall layer structures? First, from the view-point of CLg theory in which, for rotational fluctuating fields in strong shear, differential pseudomomentum plays a key role [17], we see in Fig. 8 that the differential is largely negative and confined to the sublayer and buffer layer regions, so instability would likely occur there. Were the fluctuating field due to a discrete spectrum of waves then instability to streamwise structure would be determined by the Craik-Phillips-Shen criterion [10, 11, 43], but not clear is how to apply that criterion when the spectrum is continuous. That said, the generic rotational wave and shear fields considered by [11] indicate that instability to streamwise vortices is likely; the question then is whether those structures bear resemblance to the ones observed?

To find out, we use strong shear CLg theory [8, 17, 43] to describe periodic Poiseuille flow and solve for the linear steady states which determine the stability boundary to the formation of streamwise vortices. As plotted in Fig. 9, the boundary depicts the streak spacing  $L$  depicted by two vortices against  $Re_\tau$ . Included therein are asymptotes for instability to two- and three-dimensional waves [63], the later of which is closely consistent with our  $Re_\tau = 63.5$  onset boundary to streamwise vortices as we would expect. Included also are the spacings of two rolls found numerically in periodic Poiseuille flow at  $Re_\tau = 80$  [41], which are within our stability boundary and thus consistent with our findings. Finally, we note that onset, depicted by the nose of the curves, occurs at  $L \approx 120$  wall units, a value near the circa 100 mean streak spacing in turbulent boundary layers first reported by Kline *et al* [66] and observed widely since. Thus while multiple mechanisms likely act to realize streamwise vortices, the structure depicted by the CLg instability mechanism is consistent that ubiquitous in the sub- and buffer-layer. CLg will also act in the log region but is likely less influential there because the drift and pseudomomentum are weaker there relative to the mean flow. Nevertheless they will still act to redistribute mean vorticity.

## ACKNOWLEDGMENTS

My thanks to Joseph Klewicki and Philip Hall for insightful discussions. This work was partially supported

by the U.S. National Science Foundation through grant

OCE-0116921 and by the Australian Research Council through grant DP1093517.

- 
- [1] M. E. McIntyre, *J. Fluid Mech.* **106**, 331 (1981).
- [2] D. G. Andrews and M. E. McIntyre, *J. Fluid Mech.* **89**, 609 (1978).
- [3] W. R. C. Phillips, *J. Fluid Mech.* **430**, 209 (2001).
- [4] G. G. Stokes, *Trans. Camb. Phil. Soc.* **8**, 441 (1847).
- [5] W. R. C. Phillips and Z. Wu, *J. Fluid Mech.* **272**, 235 (1994).
- [6] W. R. C. Phillips, A. Dai, and K. K. Tjan, *J. Fluid Mech.* **660**, 221 (2010).
- [7] N. Riley, *Ann. Rev. Fluid Mech.* **33**, 43 (2001).
- [8] W. R. C. Phillips and A. Dai, *J. Fluid Mech.* **743**, 141 (2014).
- [9] M. S. Longuet-Higgins, *Phil. Trans. R. Soc. Lond.* **245**, 535 (1953).
- [10] A. D. D. Craik, *J. Fluid Mech.* **125**, 37 (1982).
- [11] W. R. C. Phillips and Q. Shen, *Stud. Appl. Math.* **96**, 143 (1996).
- [12] A. D. D. Craik and S. Leibovich, *J. Fluid Mech.* **73**, 401 (1976).
- [13] J. L. Lumley, *Stokes drift in a turbulent boundary layer*, Tech. Rep. FDA-86-03 (Cornell University, 1986).
- [14] W. R. C. Phillips, in *Near wall turbulence: Zoran Zaric Memorial Seminar* (Hemisphere, 1988) p. 736.
- [15] W. R. C. Phillips, *Appl. Mech. Rev.* **43**, S227 (1990).
- [16] A. D. D. Craik, *J. Fluid Mech.* **125**, 27 (1982).
- [17] W. R. C. Phillips, *Stud. Appl. Math.* **101**, 23 (1998).
- [18] W. R. C. Phillips, *Phys. Fluids* **12**, 2056 (2000).
- [19] R. H. Kraichnan, *Phys. Fluids* (1958-1988) **8**, 575 (1965).
- [20] R. H. Kraichnan, *Phys. Fluids* (1958-1988) **11**, 265 (1968).
- [21] R. H. Kraichnan, *J. Fluid Mech.* **81**, 385 (1977).
- [22] R. H. Kraichnan, *J. Fluid Mech.* **77**, 753 (1976).
- [23] D. D. Holm, *Chaos* **12**, 518 (2002).
- [24] R. H. Kraichnan, *J. Fluid Mech.* **83**, 349 (1977).
- [25] S. A. Orszag and L. C. Kells, *J. Fluid Mech.* **96**, 159 (1980).
- [26] B. L. Rozhdestvensky and I. N. Simakin, *J. Fluid Mech.* **147**, 261 (1984).
- [27] L. Keefe, P. Moin, and J. Kim, *J. Fluid Mech.* **242**, 1 (1992).
- [28] F. Waleffe, *Stud. Appl. Math.* **95**, 319 (1995).
- [29] J. M. Hamilton, J. Kim, and F. Waleffe, *J. Fluid Mech.* **287**, 317 (1995).
- [30] F. Waleffe, *Phys. Rev. Lett.* **81**, 4140 (1998).
- [31] J. Wang, J. Gibson, and F. Waleffe, *Phys. Rev. Lett.* **98**, 204501 (2007).
- [32] F. Waleffe, *Phys. Fluids* (1994-present) **9**, 883 (1997).
- [33] F. Waleffe, *Phys. Fluids* (1994-present) **15**, 1517 (2003).
- [34] M. Nagata, *J. Fluid Mech.* **217**, 519 (1990).
- [35] P. Hall and F. Smith, *Proc. R. Soc. Lond. A* **417**, 255 (1988).
- [36] P. Hall and F. Smith, *Euro. J. Mech. B/Fluids* **8**, 179 (1989).
- [37] J. Bennett, P. Hall, and F. T. Smith, *J. Fluid Mech.* **223**, 475 (1991).
- [38] P. Hall and S. Sherwin, *J. Fluid Mech.* **661**, 178 (2010).
- [39] K. Deguchi and P. Hall, *J. Fluid Mech.* **750**, 99 (2014).
- [40] J. Jimnez and P. Moin, *J. Fluid Mech.* **225**, 213 (1991).
- [41] L. Sirovich, K. S. Ball, and L. R. Keefe, *Phys. Fluids A* **2**, 2217 (1990).
- [42] W. R. C. Phillips, in *Nonlinear Instability, Chaos and Turbulence*, edited by L. Debnath and D. Riahi (WIT Press, 1998) pp. 277–299.
- [43] W. R. C. Phillips, in *Wind-Over-Waves II: Forecasting and Fundamentals of Applications*, edited by S. Sajjadi and J. Hunt (Horwood Pub, 2003) pp. 157–167.
- [44] S. Leibovich, in *Studies in Turbulence*, edited by S. S. T. Gatski and G. Speziale (Springer, 1992) pp. 387–411.
- [45] W. R. C. Phillips, Z. Wu, and J. L. Lumley, *J. Fluid Mech.* **326**, 321 (1996).
- [46] W. R. C. Phillips, *J. Fluid Mech.* **525**, 215 (2005).
- [47] M. Lee and R. D. Moser, *J. Fluid Mech.* **774**, 395 (2015).
- [48] A. Townsend, *The Structure of Turbulent Shear Flow*, 2nd ed. (Cambridge University Press, 1976).
- [49] A. J. Favre, J. J. Gaviglio, and R. Dumas, *J. Fluid Mech.* **2**, 313 (1957).
- [50] J. Kim and F. Hussain, *Phys. Fluids* **5**, 695 (1993).
- [51] L. S. G. Kovasznay, *J. Aero. Sci.* **20**, 657 (1953).
- [52] S. Corrsin, in *Atmospheric diffusion and air pollution*, edited by F. N. Frenkiel and P. A. Sheppard (Academic, New York, 1959) pp. 441–446.
- [53] R. H. Kraichnan, *J. Fluid Mech.* **5**, 497 (1959).
- [54] W. R. C. Phillips, *Phys. Fluids* **30**, 2354 (1987).
- [55] W. R. C. Phillips and J. T. Ratnanather, *Phys. Fluids* **2**, 427 (1990).
- [56] W. R. C. Phillips, *Appl. Sci. Res.* **52**, 279 (1994).
- [57] J. Kim, P. Moin, and R. Moser, *J. Fluid Mech.* **177**, 133 (1987).
- [58] R. D. Moser, J. Kim, and N. N. Mansour, *Phys. Fluids* **11**, 943 (1999).
- [59] J. C. Del Alamo, J. Jiménez, P. Zandonade, and R. D. Moser, *J. Fluid Mech.* **500**, 135 (2004).
- [60] S. Hoyas and J. Jiménez, *Phys. Fluids* **18**, 011702 (2006).
- [61] A. Lozano-Duran and J. Jiménez, *Phys. Fluids* **26**, 011702 (2014).
- [62] I. Marusic, J. P. Monty, M. Hultmark, and A. J. Smits, *J. Fluid Mech.* **716**, R3 (2013).
- [63] S. A. Orszag and A. T. Patera, *J. Fluid Mech.* **128**, 347 (1983).
- [64] K. R. Sreenivasan and A. Sahay, in *Self-Sustaining Mechanisms of Wall Turbulence*, edited by R. Panton (Computational Mechanics Publications, Southampton, UK., 1997) pp. 253–272.
- [65] K. Deguchi and P. Hall, *J. Fluid Mech.* **752**, 602 (2014).
- [66] S. J. Kline, W. C. Reynolds, F. A. Schraub, and P. W. Runstadler, *J. Fluid Mech.* **30**, 741 (1967).